Chapter 8
Inorganic Acid Doped Polyaniline Based Carbon Monoxide (Co) Sensor

Muktikanta Panigrahi [1, *], Basudam Adhikari [1]

[1] Materials Science Centre, Indian Institute of Technology, Kharagpur, West Bengal, India

*Corresponding author: muktikanta2@gmail.com

Abstract

Simple *in situ* chemical oxidation method was employed to prepare different molar of HCl doped DL−PLA/PANI composites using AnHCl as precursor. Surface morphology, ATR−FTIR, UV−Visible, and band gap were studied. PANI nanowires with different diameter and smooth surface were observed for composites. The lowest direct band gap was found to be 1.68 eV for 2 (M) HCl doped DL−PLA/PANI. DC conductivity at room temperature was measured and followed the ohmic behaviour. The calculated highest DC conductivity at room temperature was found to be 0.1628 × 10^{-2} (S/cm) for 2 (M) HCl doped DL−PLA/PANI. Temperature variation (70−300 K) DC conductivity without magnetic field of as prepared composites was analysed using linear four probe techniques and showed semiconducting nature. The conductivity in the range of temperature (70−300 K) follows 3D VRH hopping mechanism. In kivelson model, the exponents are increased with increasing dopant concentration and was obeyed the power law. MR of the prepared DL−PLA/PANI composite films is strongly dependent on temperature, magnetic field, and concentration of HCl dopant. Negative MR is discussed in terms of a wave function−shrinkage effect on hopping conduction. In addition, we were discussed the response of carbon monoxide (CO) gas with polyaniline-based sensor materials.

Keywords: Composite, Nanofiber, Band gap, DC conductivity, Magnetoconductivity, Carbon monoxide Sensor

Introduction

The past few decades has witnessed rapid growth in research on conjugated polymer nanostructures, which has been driven by their unique electrochemical and

Muktikanta Panigrahi, Basudam Adhikari, *Inorganic Acid Doped Polyaniline Based Carbon Monoxide (Co) Sensor*,
https://doi.org/10.34256/ioriip2128

electronic properties as well as by the processing advantages of polymers relative to other electronic materials. The applications of conducting polymer nanostructures have been recently reviewed [1, 2]. Recently, conducting polymer nanowire and nanotube have been proposed as active materials for various potential commercial applications such as antistatic shielding, light emitting diodes (LED), supercapacitors, rechargeable batteries, artificial muscles, corrosion inhibitors and sensors [3-11].

In the conducting polymer family, PANI is one of the members with good environmental and thermal stability along with easy processing and oxidation−reduction mechanism, high conductivity [12-14]. Notwithstanding above advantages, PANI film has certain limit such as brittleness and moisture sensitivity that creates problems for its commercial applications. In various ways, researcher was tried to improve their stability. One of the effective ways was found in literature to improve the stability of PANI salt by making in composite form with thermoplastic polymer act as stabiliser [13]. A variety of doped PANI composite have been prepared using many types of thermoplastic polymers such as poly (methyl methacrylate), polyvinyl chloride, polystyrene and polyurethane and their conductivity was studied with and without magnetic field at room temperature and temperature variation (50−300 K) [15-18].

For future prospectus, researchers are introduced biodegradable polymers into the preparation conducting films with conducting polymer like PANI and polypyrrole (PPy).This is because biodegradable polymers have polar character (presence of polar groups) and conducting polymers have also polar character. The covalent interaction may be happened after composite preparation. Few reports are reported on composite that was made from biodegradable polymer and conducting polymers [19-21]. DL−PLA is one of the biodegradable polymers in biodegradable family. We chose DL−PLA biodegradable thermoplastic polymer has reported to the comparable good mechanical, bioresrorable, compatibility, surface properties with other biodegradable polymer and covalent interaction with conducting polymers. These materials can be used in different fields such as biosensor [21], intelligent scaffold materials [19], biochips [20] and gas sensing materials (present work).

It is well known that conductivity is key parameter for conducting polymer throughout its back bone. Conductivity was occurred only for charge transport phenomena in intra – and inters chains of the conducting polymer. For gas sensing applications, conductivity in terms of resistance change plays vital role and therefore, it is important to understand the charge transport in nanofibers because the charge transport mechanisms can have important consequences in term of the sensor signal to noise ratio. Some reports of thin film [22] and nanowires [23] are reported the complex electronic behaviour. The present scenario comes from structure of polymer. The polymeric structure mainly depends on synthetic condition, doping level, and balancing counter ions. Till now, the research is going on the study of transport behaviour throughout the conducting polymer. Such behaviour are found to be variety ways as electrical conductivity, magnetoresistance, frequency dependent conductivity, magnetic susceptibility, thermoelectric power have been intensively explored in the

last two decades [24, 25]. Out of above electrical properties, magnetoresistance is one important electrical property and that has been used to apply in various fields such as magnetic field sensor for studying high T_c – superconductor taps [26], vibration measurements in MEMS [26], manufacturing magnetocoupler device [26], detecting DNA or Protein binding to capture molecules in a surface layer [26]. Various reports have been studied magnetoresistance with temperature variation at particular magnetic field [27-29] or various magnetic fields at particular temperature [27-29] studying conducting behaviour. Different important parameters such as density of states (N_F), localization length (L_{loc}), characteristic temperature (T), hopping distance (R_{hop}) and hopping energy (Δ_{hop}) related to conduction mechanism were estimated for studying magnetoresistance with temperature variation at particular magnetic field.

Our purpose is to prepare an environmentally stable PANI composite that would show considerable good electrical properties. Also, it can be potential for sensor and other electronic applications. Looking for the above properties, biodegradable polymer such as poly (lactide) (DL-PLA) polymer is one of the thermoplastic polymers, which is used to prepare novel conductive material. It has good electrical conductivity, good durability, good environmental stability and easy processability.

In this input, author investigates the ethanol sensing of 2M HCl doped DL−PLA/PANI composites (different sized nanofibers) are prepared by *in situ* polymerization method. Also, the DC conductivity at room temperature and with temperature variation (presence and absence of magnetic field), response of CO, ATR−FTIR spectra, and UV−Visible with direct band gap has been studied.

Experimental Section

Chemicals And Materials

Laboratory grade chemicals such as aniline hydrochloride (AnHCl), hydrochloric acid (HCl), chloroform ($CHCl_3$), and ammonium perdisulphate (APS) are purchased from Merck, India. DL−PLA polymer is procured from Cargill Dow Bair; US−NE. Distilled water is used throughout the preparation of doped PANI composites.

DL−PLA films are prepared by solution casting technique. Both DL−PLA polymer (3 g) and $CHCl_3$ (30 mL) are taken as components during the DL−PLA film preparation. DL−PLA polymers are put in $CHCl_3$ contained beaker (100 mL). The mixture is stirred (3 h) by magnetic stirrer. It is observed that transparent soluble product is formed. The products are poured into ptridish (10 cm diameter). After $CHCl_3$ evaporation, films are removed from ptridish and cut into small pieces (1.5 cm × 1.5 cm). The schematic representation of DL−PLA film preparation is mentioned as flow chart and presented in Scheme A.

At ambient condition, various molar of HCl doped DL−PLA/PANI composites are prepared by *in situ* method through chemical oxidation polymerization route from AnHCl (monomer) and DL−PLA film as substrate. 0.03 moles (2.59 g)

AnHCl is added to 50 mL of 1 (M) HCl in 250 mL conical flask, called “solution A”.

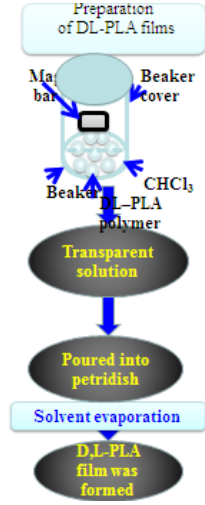

Scheme A. The schematic representation of detail preparation of DL−PLA film is mentioned as flow chart and presented in Scheme A

DL−PLA films (1 cm × 1 cm) is dipped to “solution A” and stirred for 12 h. 0.045 moles (10.24 g) of APS was put to 50 mL of 1(M) HCl to form “solution B”. To the “solution A”, “solution B” is added drop wise for 1 h to form “solution C” and continued the stirring to 4 h. The polymerization is carried out in “solution C”. The color of “solution C” and DL−PLA films became light green to dark green. The reaction mixture is stayed overnight. The resulting composites are washed with deionised water several times followed by dried in air for 6 h [30].

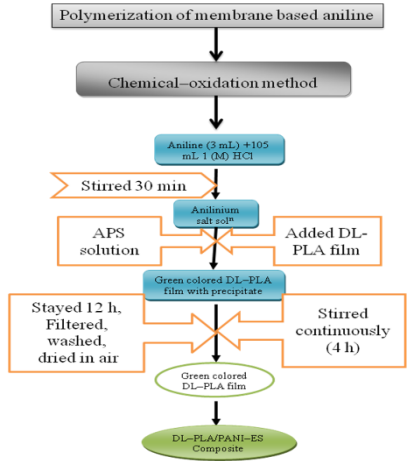

Scheme B. The flow chart of preparation of HCl doped DL-PLA/PANI-ES composite

For comparison study, 2(M) −, and 3(M) – HCl doped DL−PLA/PANI composites are also prepared under similar conditions to those mention above. The flow chart of the preparations is illustrated in Scheme B.

Characterization Section

Surface morphologies of the as prepared materials are analyzed by scanning electron microscope (SEM, Carl Zeiss Supra 40). All samples are needed gold coating before doing SEM measurements.

For studying electronic transitions of all the prepared materials are needed UV−Visible (Micropack UV−VIS−NIR, DH 2000) spectral analyses. Band gap is estimated by Tauc expression.

In support of ATR−FTIR spectra, functional groups of all as prepared materials are recorded on a Thermo Nicolt Nexus 870 spectrophotometer in the range 400-4000 cm^{-1}.

Both room− and low temperature DC conductivity of all as prepared composites are measured using a linear four probe technique. Also, Magnetoresistivity is measured using a linear four probe technique. Magnetoresistivity is investigated using a helium compressor (HC) (model HC-4E1)-sumitomo cryostat (Model Gains Research CO, INC) equipped with 0.8 T superconducting magnet (Lake shore electromagnet). Lake shore 331 temperature controller is used. Magnetoresistivity measurements are performed at 0.5T with varying temperature 50-300 K temperatures range using a computer controlling measuring system. In above electrical experiments, prepared film samples (thickness~0.51 mm) are contacted with conducting silver paste. A constant current (I) from a current source (Keithley 220 programmable current source) is allowed to pass through two terminals leads of four probe and the voltage (v) across the other two leads is measured using a multimeter (2182 NANOVOLTAMETER Keithley).

Results and Discussion

Figure 1 shows the variety of SEM images of prepared materials such as neat DL−PLA, neat 1 (M) HCl−doped PANI films, and PANI nanowires on DL−PLA film at room temperature. Smooth surface was observed in neat DL−PLA film (Figure 1 A) below 1 kX magnification whereas neat PANI and all HCl doped composites (Figure 1 B, C, D and E) have fibrous structure was observed in magnified SEM images having diameter in nanoregime, so called nanofiber. Non−uniformly distribution of nanofiber was observed in HCl doped composites and HCl doped PANI salt film. The average diameter of as prepared HCl doped materials was found to be 185.3 nm for HCl doped 1(M) DL−PLA/PANI composite, 165.1 nm for HCl doped 2(M) DL−PLA/PANI composite, and 211. 3 nm for HCl doped 3(M) DL−PLA/PANI

composite, respectively. The fiber like morphology was observed after polymerization start. This may be happened due to the reaction of hydrogenium ion from HCl and anillium salt with ester group present in DL−PLA film with drop wise addition of APS (oxidant) solution on a solution that contain anillium salt with DL−PLA (monomer and HCl treated) film. The formation of Nanofiberic structure is favourable for the sensor application due to increase in surface area of PANI. This

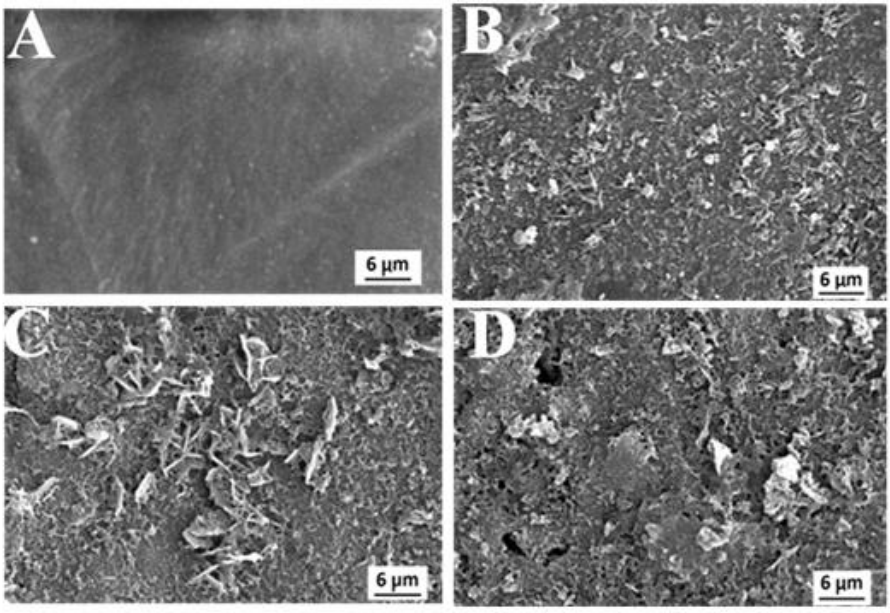

high surface area provides fast diffusion of gas molecules into the PANI nanofibers.

Figure 1. shows the variety of SEM images of prepared materials such as neat DL−PLA, 1 (M) HCl-doped DL-PLA/PANI composite (B), 2 (M) HCl-doped DL-PLA/PANI composite (C), and 3 (M) HCl-doped DL-PLA/PANI composite (D) films

Chemical structure of prepared materials was observed by analysis of ATR−FTIR spectra. Figure 2 indicates the ATR−FTIR spectra of DL−PLA, PANI−ES (1 M) and all prepared conductive composites. All the characteristic absorption peak positions of all prepared materials and its assignments are given in Table 1. The ATR−FTIR spectra of DL−PLA film was presented in Figure 2 (A). The variety of absorption bands of DL−PLA was found at 2995, 2944, 1759, 1616 and 1216 cm^{-1}, respectively. That bands have been attributed to C−H stretching, C=O stretching, C−O stretching of ester and C−O−C stretching vibration, respectively. The stretching vibration of C−H deformation band of DL−PLA polymer was found at 1453, 1361 and 1363 cm^{-1} [31]

This represents the characteristic absorption features of DL−PLA polymer and that are retained in the prepared DL−PLA film. An ATR−FTIR spectrum of HCl

doped PANI was observed in Figure 2 (C).

Table 1 for ATR−FTIR peak positions and peak assignments of as−prepared materials

Peak positions (cm^{-1})					
DL−PLA	**PANI ES**	**DL−PLA/PANI 1 (M) HCl**	**DL−PLA/PANI 2 (M) HCl**	**DL−PLA/PANI 3 (M) HCl**	**Peak assignments**
2995		2995	2969, 2968	2968	
2944	---	2944	2922	2925	CH stret.
---	3227 (W)	3287	3289	3295	NH stret.
	3429 (S)	---	---	---	NH stret.
1759	---	1739	1725	1725	C=O stret.
1616	---	1616	1652	1652	C − O stret.
---	1564	1570	1530	1530	Quinoid stret.
---	1479	1482	1451	1454	Benzoid stret.
---	1116	1042	1070	1070	C=N stret.
1216	---	1214	1226	1226	C − O − C stret.
1453	---	1434	1411	1411	
1363	---	1361	1451	1454	
1361	---	---	1371	1373	
			1338	1345	CH − deform.

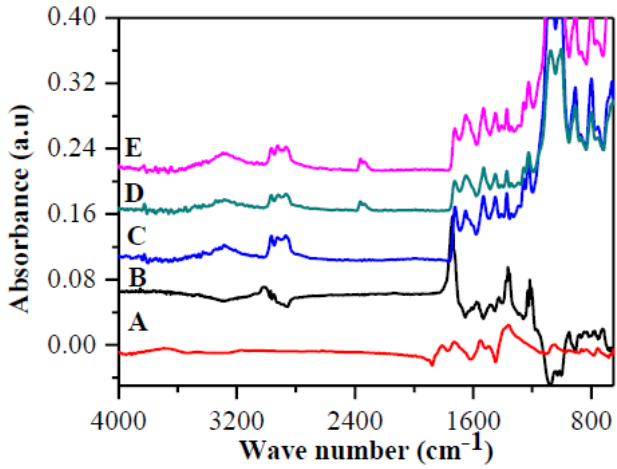

Figure 2. ATR−FTIR spectra of pristine DL−PLA ‘A’, PANI ES film ‘B’, DL−PLA/PANI 1 (M) HCl ‘C’, DL−PLA/PANI 2 (M) HCl ‘D’, and DL−PLA/PANI 3 (M) HCl ‘E’

The bands are found at 1554 cm^{-1} for quinoid, 1475 cm^{-1} for benzoid, and 1108 for C=N cm^{-1} stretching, respectively [32].This corresponds to the oxidation of PANI. The ATR−FTIR spectra of all composites are presented in Figure 2 (C), (D), and (E). Considering all the band features of as−prepared composites and comparing

with the band features of DL−PLA and HCl doped PANI, we conclude that salt form PANI is formed on DL−PLA film. From Table 1, it is observed that N−H bands of HCl−doped DL−PLA/PANI 1(M), HCl doped DL−PLA/PANI 2(M), HCl doped DL−PLA/PANI 3(M) appeared at 3291, 3289, and 3295 cm^{-1}, respectively. The variation of N−H stretching bands between prepared composites was strongly depended on concentration of HCl. The C=N, C=O, C−O and C−O−C stretching bands do not change significantly.

Variety of electronic transitions of as−prepared materials was established by studying UV−Visible spectra. This spectrum was existed in Figure 3. The band positions and band assignments of each prepared materials are mentioned in Table 2. From Figure 3 (A), it is noticed that no electronic transitions are found in DL−PLA film [33].

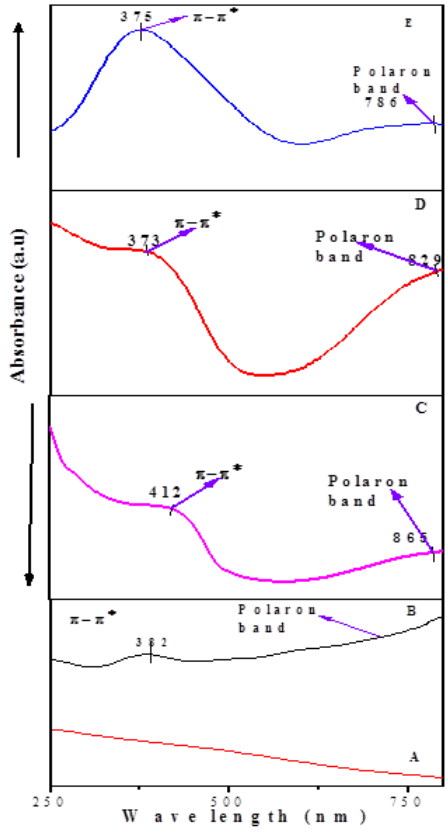

Figure 3 UV−Visible spectra of pristine DL−PLA 'A', PANI ES film 'B', DL−PLA/ PANI 1 (M) HCl 'C', DL−PLA/PANI 2 (M) HCl 'D', and DL−PLA/PANI 3 (M) HCl 'E'

It is mentioned from literature that PANI−ES shows various types of

electronic transitions such as $\pi-\pi^*$ of benzene ring, polaron to π^*, benzoid to quinoid ring and polaron transition, respectively [34]. An UV−Visible spectrum of HCl doped PANI (1 M) film is indicated in Figure 3 (B). Polaron band and $\pi-\pi^*$ were found at 382 nm and >600 nm. This represented as the oxidation form PANI [27]. All the as prepared composites were generally showed in Figure 3 two types of transitions such as π to localised polaron band transition and $\pi-\pi^*$ transition of benzoid ring. The peak positions were found 865 nm and 412 nm for HCl doped DL−PLA/PANI (1 M), 829 nm and 373 nm for HCl doped DL−PLA/PANI (2 M), and 786 nm and 375 nm for HCl doped DL−PLA/PANI (3 M), respectively. Both $\pi-\pi^*$ transition of benzoid ring and polaron band are suggest to the presence of aniline unit and oxidation unit in emeraldine salt form of composite films.

Electronic transitions were occurred between two bands and that happened after photon absorption. From many literatures [35] was mentioned that the photon absorption of organic semiconductor is followed by Tauc expression as

$$(\alpha h\nu) = A\left(h\nu - \mathrm{E}_g\right)^n \qquad (2)$$

Where α = Optical absorption co−efficient, $h\upsilon$ = photon energy, E_g = Energy gap calculated from graph, A = absorption constant, n = Represents types of transition occurs. If n = 2 indicated allowed indirect transitions and $n=\frac{1}{2}$ indicated allowed direct transitions.

Table 2. UV−Visible band positions and its assignments of indicated materials.

Materials Identification	Peak positions (nm)		Band gap (Eg) in eV
	$\pi-\pi^*$	Polaron band	
DL−PLA	---	---	---
PANI ES film	382	>650	1.08
DL−PLA/PANI (1M HCl doped)	412	>865	>865
DL−PLA/PANI (2M HCl doped)	373	>829	1.68
DL−PLA/PANI (3M HCl doped)	375	>786	1.82

Note: ‘M’ stands for molar, ‘nm’ stands for nanometre and ‘eV’ stands for electron–volt

For direct electronic transition, plot was made between $(\alpha h\upsilon)^2$ and $h\upsilon$. From the plot, to extrapolate the linear portion of it to α = 0 value to obtained corresponding direct band gap. Direct allowed transitions, all the prepared composites are shown in Figure 4 and its (band gap) values are presented in Table 3. It is observed from Table 3, 2 (M) HCl doped of DL−PLA/PANI composite have obtained lowest direct band gap value as compared to other HCl doped composites. The reduction in band gap

occurred due to the incorporation of H^+ ion concentration into the polymer chain; but there is certain limit and that affect the density of states, which is more into the visible region as compared to excess dopant used for composite preparation [35].

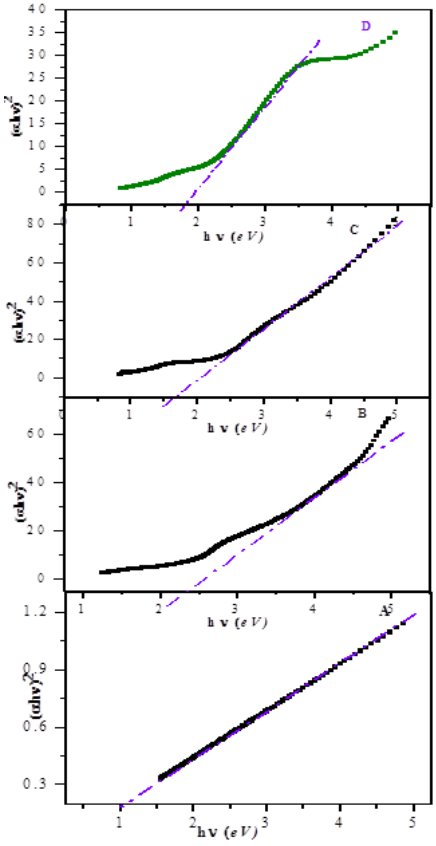

Figure 4. Estimation of direct band gap using Tauc expression of pristine PANI ES film 'A', DL−PLA/PANI 1 (M) HCl 'B', DL−PLA/PANI 2 (M) HCl 'C', and DL−PLA/ PANI 3 (M) HCl 'D'

Conductivity is an important spirit for conducting materials. This character was measured by various ways. Linear four probe technique is one technique out of them and this technique was favoured for the researchers due to the minimization of voltage drop.

The DC conductivity of as prepared composites was measured using linear four probe technique and the expression is shown below [36].

$$\rho = 2\pi S\left(\frac{V}{I}\right) \qquad (3)$$

$$\sigma = \frac{1}{\rho}$$ and (4)

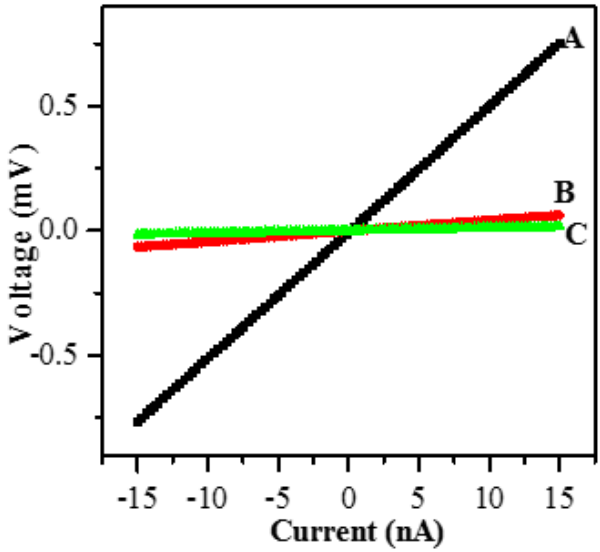

Figure 5. Room temperature DC conductivity of HCl doped 1 (M) 'A'−, 2 (M) 'C'−, 3 (M) 'B'–DL−PLA/PANI composites, respectively.

ρ = resistivity, S = distance between two consecutive probes (0.15 cm), I be the applied current in the four probe system (nA) and V be the corresponding output voltage in (mV). The room temperature $I-V$ characteristics of HCl doped DL−PLA/PANI composites were shown in Figure 5. This indicates that the $I-V$ characteristics show linear behaviour (I and V) and passing through origin (after linear fit). This nature follows similar to the ohmic behaviour and is reported as [36]. The average (av.) DC conductivity values of HCl doped DL−PLA/PANI composites, and DL−PLA polymer film were presented in Table 3. It is cleared from the Table 3, the measured DC conductivity at room temperature of DL−PLA film are found to be 6.07×10^{-15} S/cm and it is pointing to an insulating materials [37]. Also, from Table 3 it is found that the av. DC conductivity of 2(M) HCl doped DL−PLA/PANI composites are found to be higher than rest of prepared composites. Conductivity may obtain due to the mobility of charge carrier. This carrier mobility mainly depends on the presence of reduced unit in PANI structure and that was happened due to the improvement of PANI salt structure at 2 (M) HCl doped prepared composite [38]. But excesses dopant concentration, that create a barrier for their charge transport in intra− and inter−PANI chains. Hence, the results are agreed with literature [38].

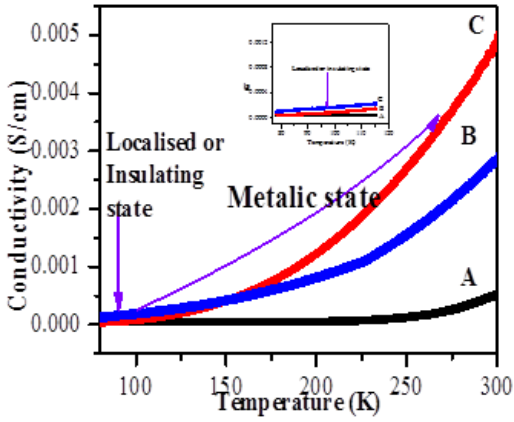

Figure 6. Temperature dependent DC conductivity of HCl doped 1(M) 'A'−, 3(M) 'B'−,2(M) 'C'−DL−PLA/PANI composites, respectively and 70−115 K for localised state or insulating state and 115−300 K for metallic state are observed.

Until, charge transport process is difficult to understand of conducting materials. For understanding of conduction mechanism of as prepared composites, low temperature DC conductivity experiments were performed. Temperature variation (78−300 K) DC conductivity of HCl doped DL−PLA/PANI composites were showed in Figure 6. It is observed from Figure 6 that the conductivity of as prepared composites is proportionally increased with increase in temperature. Analogous nature was found from semiconducting materials [36].

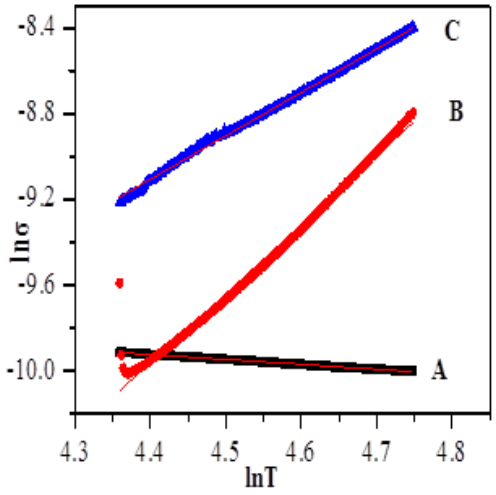

Figure 7. Temperature dependent DC conductivity in logarithmic scale following Kivelson model of HCl doped 1(M) 'A'−, 3(M) 'B'−,2(M) 'C'−DL−PLA/PANI composites, respectively and slopes are corresponding to the exponent.

Hence, it is called as organic semiconductor. The temperature dependence of electronic conductivity was obtained from prepared nanofibers with different diameter. Figures 6 are shown the conductivity of all prepared composite samples and were exhibited two characters [27]. One is metallic character and that was observed in the temperature range 115−300 K. Other one is localised behaviour and that was found below 115 K. This behavior agrees with the Bloch−Gru¨neisen theory on the electron−acoustic phonon scattering mechanism. On the other hand, the smaller sample shows two distinct characteristics for the electron transport.

Different scattering mechanism was involved to determine the temperature dependence conductivity. At high temperatures (T > 115 K), the scattering mechanism seems to be predominant and the conductivity rises with increasing temperature (metallic phase) [27]. As the temperature is lowered, phonon scattering mechanisms become predominant [27], giving rise to a distinct temperature−dependent conductivity for T < 115 K, which explains in part the general features of the curve presented in Figure 6. At low temperature regime, the scattering mechanism can be related with the size of the nanofibers: as the nanofibers cross section decreases, the boundary scattering becomes relatively more important than for larger fibers because a larger portion of the carriers are located near the fibers boundary. Then (1) for small−dimension nanofibers, the disorder coming from processes like collisions with the boundaries [39, 40] provides the necessary disorder to randomize electron energy, resulting in a localized character for the transport; (2) this will increase the electron−electron interaction as well [41]. It is important to emphasize that the conductivity below 110 K is not related with strong localization: the disorder from boundary scattering, randomizing the electron potential, is not enough to promote strong localization. In fact, successive attempts in order to distinguish an activation law (Arrhenius model) or a variable range hopping (VRH) behaviour have failed [42-45].

In order to explain the current transport i.e. electron−electron or electron phonon or mixed charge carrier in localised state in the temperature range T < 115 K (below the solid line) was presented in Figure 7. The experimental data for T < 115 K was the best fitted, such model called Kivelson model [45]. According to this model, the temperature dependence conductivity is expressed as [45]

$$\sigma(T) = A(T^n) \qquad (5)$$

Where A is some constant and n is the exponent. According to this model, we plotted lnσ *vs.* lnT. The 'n' is equal to the slope of the straight line. The values of 'n' were found to be 0.229 eV, 2.72 eV, and 3.316 eV for 1 (M) DL−PLA/PANI composite, for 2 (M) DL−PLA/PANI composite, for 3 (M) DL−PLA/PANI composite, respectively. This value is deviate the values of one dimensional electron−electron scattering and this should be addressed mixed charge carrier below the 115 K [45].

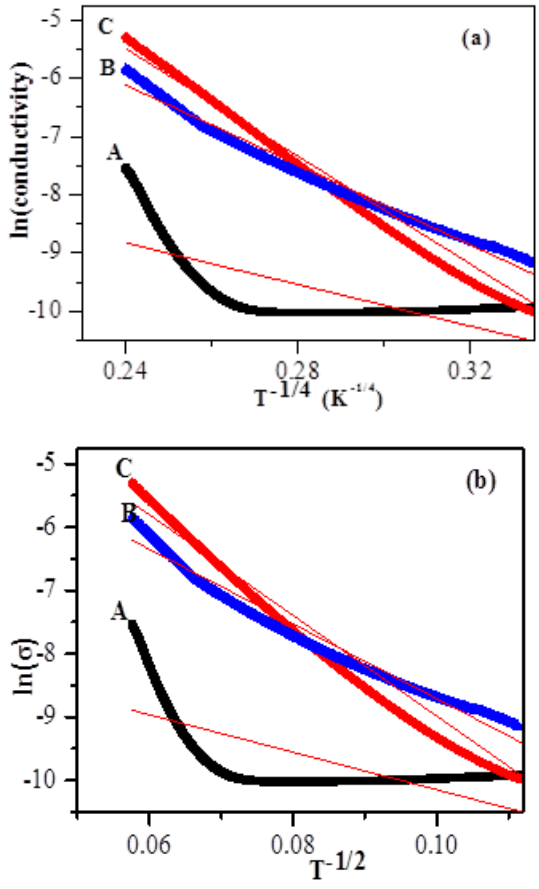

Figure 8. Temperature dependent DC conductivity of HCl doped 1 (M) 'A'–, 2 (M) 'B'–, 3 (M) 'C'–DL−PLA/PANI composite, respectively and showed (a) for 3D (a) − and 1D (b) −VRH model.

Variety of models was proposed to understand the conduction process of the conducting polymers. Generally, Mott's variable range hoping (Mott's VRH) model has been applied to organic semiconductor for understanding the hopping mechanism for conduction and that can be observed from temperature dependent conductivity. In this report, we mentioned the temperature dependence (78−300 K) conductivity (Figure 8) for studying Mott's VRH form of HCl doped DL−PLA/PANI composites. The temperature dependence DC conductivity as follows the eq^{n} (5) [42-45] and this is called Mott's expression.

$$\sigma = \sigma_0 \exp\left(-\frac{T_0}{T}\right)^X \qquad (6)$$

Where T_0 is the Mott characteristic temperature and σ_0 the limiting value of conductivity at infinite temperature and the exponent 'r' is related to the dimensionality of the transport process using the relation $x = \frac{1}{(1+d)}$, where d =1, 2 and 3 for one−, two− and three−dimensional (1D, 2D and 3D) transport process, respectively.

The 3D VRH plots on measured ln (conductivity) *vs.* $T^{-1/4}$ for HCl doped DL−PLA/PANI composites in the temperature range 78−300 K were shown in Figure 8 (a). This conductivity data were well linearly fitted to the 3D conduction process. Similarly, 1D−VRH plots were shown in Figure 8 (b). It is cleared from all VRH plots, Mott's 3D VRH model of 2(M) HCl doped DL−PLA/PANI composite fits better into the experimental data than that of other VRH model. The linearly fit behaviour is observed from regression values and these values are presented in Table 3. Higher the regression values (i.e. close to unity) suggest the more charge carrier can hop in intra– and inter–hopping processes because of PANI chain structure, supporting the reported literatures [42-45]. In the 3D−VRH model, the temperature dependence of DC−conductivity can be presented in equation (2)

$$\sigma = \sigma_0 \exp\left[-\left(\frac{T_0}{T}\right)^{\frac{1}{4}}\right] \qquad (7)$$

as can be seen in Figure 8 (a), the linear dependence of $\ln \sigma$ vs. $T^{-\frac{1}{4}}$ is well fitted. T_0 and σ_0 was also calculated from 3D−VRH plot of HCl−doped DL−PLA/PANI composites and presented in Table 3. It concluded that charge carriers could hop easily in 2 (M) HCl−doped as prepared composite than rest prepared and follow the conduction mechanism [43].

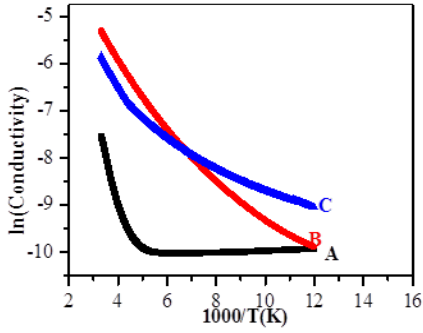

Figure 9. Plots on ln□ vs. 1000/T−1 of HCl doped 1(M) 'A'−, 3(M) 'B'−, 2(M) 'C'−DL−PLA/PANI composites, respectively and Arrhenius models are followed.

Another important model i.e. Arrhenius model was employed to estimate the activation energy (minimum amount of energy needed to hop the inter chain) of prepared composite and this model is shown in Figure 9. Accordingly, Arrhenius eq^n. is represented as a function of temperature and the electronic conductivity is inversely

related i.e. $\sigma = f\left(\frac{10^3}{T}\right)$. The following expression is investigated from literature to Arrhenius model [44] in the temperature regime 78 to 300 K.

$$\sigma = \sigma_0 \exp\left(-\frac{E_a}{kT}\right) \qquad (8)$$

Where E_a is the thermal activation energy of the electrical conduction, σ_a is a constant and that is depending on the semiconducting behaviour, T is the absolute temperature in Kelvin scale, and k is the Boltzmann constant and its value is 8.62×10^{-5} (eV/K).

From Figure 9 shows that the conductivity value does not exhibit linear dependency but markedly curved which indicates that the conductivity does not correspond to a thermally activated mechanism [44].Taking slope value obtained from plot of ln σ vs. 10^3/T (after linear fit), the activation energy was calculated and its value is found to be 0.0195 eV for HCl doped DL−PLA/PANI 1(M) composite, 0.04974 eV for HCl doped DL−PLA/PANI 2(M) composite, and 0.0334 eV for HCl doped DL−PLA/PANI 3(M) composite, respectively. This different value of activation energy was observed and this may be happened due to the formation of different nanosized PANI chains.

In addition, the temperature variation (50−300 K) resistivity of HCl−doped DL−PLA/PANI composites in the presence of magnetic field (0.5 Tesla) was plotted in Figure 10.

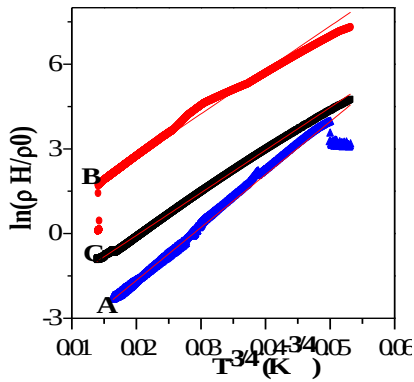

Figure 10. Plots of ln (ρH/ρ0) vs. $T^{-\frac{3}{4}}$ for HCl 1 (M) 'A'–, 2 (M) 'B'–, and 3 (M) 'C'–doped DL−PLA/PANI composites at 0.5T in the temperature range of 50–300 K. Taking slopes (from these plots), Mott's characteristic temperature (T_0), localization length, density of states, hopping distance, and hopping energy were estimated.

This characterization is very essential to support for better understanding of conduction mechanism. From this, we are calculated the important electrical parameters such as density of states *[N(E_F)]*, localization length (L_{loc}), hopping distance between the chains ($R_{hop, Mott}$), and hopping energy i.e. the energy required to

hop the electron ($^{\Delta E_{hop,Mott}}$).

From resistivity data (3D−VRH model), Mott's law is described [27] and the expression is given below.

$$\rho(T) = \rho_0 e^{\left(\frac{T_{Mott}}{T}\right)^{\frac{1}{4}}} \quad (9)$$

$$T_{Mott} = \frac{16}{\left[K_B N(E)_F L^3_{loc}\right]} \quad (10)$$

Where K_B is the Boltzmann constant; $N(E_F)$ is the density of states at the Fermi level; and L_{loc}, the localization length. T_{Mott} is an important parameter for calculation of $N(E_F)$, and L_{loc}. In 3D VRH model, we have plotted $\ln\sigma$ *vs.* $T^{-\frac{1}{4}}$ of HCl−doped DL−PLA/PANI composites and shown in Figure 8 (a). From slope of the straight line, T_{Mott} was estimated and listed in Table 3.

Table 3 Several parameters estimated from using the Band gap (direct), DC conductivity, VRH model, Power model, and Arrhenius model of prepared HCl doped DL−PLA/PANI Composite

Sample parameters	**Symbol for materials identifications**				
	A	**B**	**C**	**D**	**E**
σ (S/cm)	6.07×10^{-15}	0.910×10^{-3}	0.3115×10^{-4}	0.1628×10^{-2}	0.410×10^{-3}
σ_0	---	---	0.01057	266.93	8.12049
L_H (nm)	---	---	0.0155	0.0155	0.0155
L_{loc} (nm)	---	---	31.20	146	87.80
$N(E_F)$ (no. states/ eV/cm^3)	---	---	3.41×10^{27}	2.845×10^{23}	5.847×10^{24}
$R_{hop,Mott}$ (nm) at 300 K	---	---	102.80	1582.8	654.66
$\Delta_{hop,Mott}$ (meV at 300 (K)	---	---	56.80	186	128.54
$T_{Mott}\ (K)$	---	---	1.79×10^{6}	2.096×10^{8}	4.69×10^{7}

k = Boltzmann constant, $T_{Mott}\ (K)$ = Motts characteristics temperature in Kelvin, σ_0 = intercept value obtained from 3D VRH model, σ be the conductivity at room temperature and unit can expressed as S/cm. k (eV/K) = 8.62×10^{-5}, L_{loc} = the localization length in (nm), $N(E_F)$ = Density of states at Fermi level (no. states per electron volt per centimetre cube), $R_{hop,Mott}$ (nm) at 300 K = Mott's hoping distance in nanometre scale and the energy difference between the sites in the Mott's limits.
A, B, C, D, and E are the symbol for prepared materials identification: DL−PLA = A, PANI film (0.61 mm) = B, DL−PLA/PANI (1 M HCl doped) = C, , DL−PLA/PANI (2 M HCl doped) = D,

DL−PLA/PANI (3 M HCl doped) = E.

From magnetoresistivity data, we have plotted $\ln\left[\rho(H)/\rho(0)\right]$ *vs.* $T^{-3/4}$. The equation for magnetoresistivity with varying temperature at a particular magnetic field was shown as follows [27]

$$\ln\left[\frac{\rho(H)}{\rho_0}\right] = t\left(L_{loc}/L_H\right)^4\left(\frac{T_{Mott}}{T}\right)^{\frac{3}{4}} \tag{11}$$

Where, $t = \frac{5}{2016}$ and $L_H = \left[\frac{h}{2\pi eH}\right]^{\frac{1}{2}}$ is magnetic length, h = Planks constant (6.62×10^{-34} joule.sec), e = electronic charge (1.6×10^{-19} C), H = 0.5 T is the applied magnetic field, ρ (H) be the resistivity with magnetic field and ρ (0) is the resistivity without magnetic field. The L_{loc} can be calculated from slope of the magneto−resistivity data is shown in Figure 10.

The obtained L_{loc} is presented in Table 4. Putting $T_{0,Mott}$ and L_{loc} values in eq^n (5), (7), and (8), $N(E_F)$, (R_{hop}), and (Δ_{hop}) were calculated and was presented in Table 4. The eq^n (7) and (8), was found from literature as referred 27.

$$R_{hop,Mott} = \left(\frac{3}{8}\right)\left(\frac{T_{Mott}}{T}\right)^{\frac{1}{4}} L_{loc} \tag{12}$$

$$\Delta_{hop,Mott} = \left(\frac{1}{4}\right)\left(k_B T\right)\left(\frac{T_{Mott}}{T}\right)^{\frac{1}{4}} \tag{13}$$

By putting required parameters in the above expressions, the values of $R_{hop,Mott}$ and $\Delta_{hop,Mott}$ were calculated at 100 K and presented in Table 4. In addition, the obtained hopping parameters were found to satisfy the 3D−VRH criterions.

MC is a one of the important physical properties of conducting polymer. This property is informed to the disorderness of the materials in quantitatively. For this purpose, we performed MC measurements. Some reports are reported that weak disorder leads to a weak localization due to constructive quantum interference of time−reversed electron trajectories [46]. Below 115 K temperature, the localised character of prepared samples should be controlled by quantum interference effects, which in turn should be observed in the magnetoconductivity of the prepared nanofibers. Figure 11 shows the magnetoconductivity data obtained at 50K, 100K, 200K, and 300K temperatures, using the usual $B \perp I$ geometry (Taking I = 50 nA), with the magnetic field B ranging from 0 to 0.8 T. The presence of the electron quantum interference effects was then readily observed: (1) the increase of the conductivity with increasing magnetic field at 50K, 100K, and 200K temperature but the reverse effect was observed at 300K for HCl−doped DL−PLA/PANI (1M) composite in

Figure 11 (a)

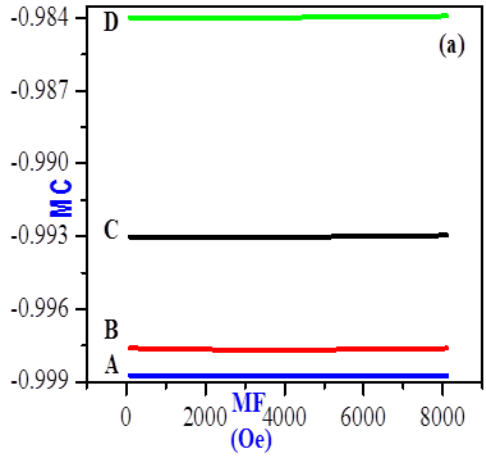

Figure 11(a) Plots on negative Magnetoconductivity vs. Magnetic field (MF) of HCl 3 (M)− 'A' at 50 K, 3 (M)− 'B' at 100 K, 3 (M)− 'C' at 200 K, and 3 (M)− 'D' at 300 K−doped DL−PLA/PANI composites, respectively.

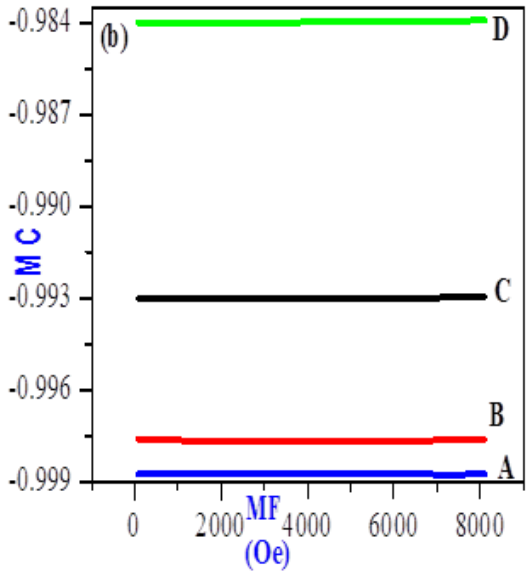

Figure 11(b) Plots on negative magnetoconductivity *vs.* Magnetic field (MF) of HCl 2 (M)− 'A' at 50 K, 2 (M)− 'B' at 100 K, 2 (M)− 'C' at 200 K, and 2 (M)− 'D' at 300 K−doped DL−PLA/PANI composites, respectively.

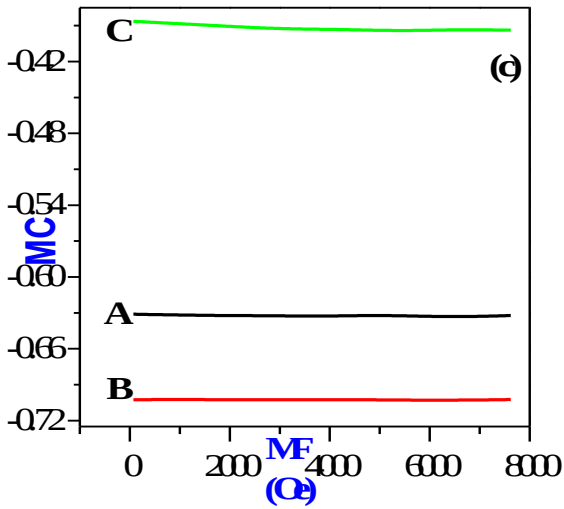

Figure 11(c) Plots on negative Magnetoconductivity vs. Magnetic field (MF) of HCl 1 (M)− 'A' at 100 K, 1 (M)− 'B' at 200 K, and 1 (M)− 'C' at 300 K−doped DL−PLA/ PANI composites, respectively.

In addition, the decrease of conductivity with increasing magnetic field at different temperature was observed in the Figure 11 (b and c) for 2 M− and 3M−HCl doped DL−PLA/PANI composites, respectively used for this experiments. The above negative MC results are agreement with the one−dimensional character of the samples [28].

Response of Carbon Monoxide (Co) Gas

Monitoring of Carbon monoxide (CO) is a key issue in the environment because of their toxic nature. Other than the toxic nature, CO is a colorless, colorless, and tasteless gas in the environment. CO is usually obtained in both sources such as natural sources and artificial sources. The major percentage of CO is come from indoors such as garages, kitchens, etc. Also, CO is produced during the combustion of engines, stoves, water heaters, generators, lanterns, and gas ranges or during burning charcoal and wood [47]. Huge amounts of CO are obtained from during the burning of any fossil fuel. Long-term with constant CO exposure is produced from automotive exhaust, smoke, and industrial sources (foundries, mills etc.) [48-52]. CO takes place following chemical reactions with hemoglobin. It can produce carboxyhemoglobin via bonding with hemoglobin, which is present in red blood cells. Due to the formation of carboxyhemoglobin, the extent of binding between the red blood cells and oxygen is reduced. Hence, the transport of oxygen in the human body decreases. This is resulted in the decrease in oxygen levels of the body and causes histotoxic hypoxia. Therefore,

it is resulting common health issues such as headache, nausea, vomiting, inertia, unconsciousness, weakness, hypotension, coma, inflammation of existing diseases, confusion, depression, hearing problems, etc. [48, 49]. Also, CO can cause for diabetes, parkinsonism, rhabdomyolysis, motion disorders. It may also cause the health issues of children and pregnant women. Inhalation of a small amount of CO over a long period of time or a large amount of CO in a short period of time can kill a person. Because of that, it is needed to monitor the toxic CO gas by best material and technology. Thus, researchers put their effort by taking many materials for their optimization. They are prepared materials using different methods and techniques. The prepared materials are used to detect this gas. The CO gas is also created in residential and household environments. So, it is very essential to develop mini or micro sensor, which is cost effective and efficient in these environments. It detects CO in parts per million (ppm) and parts per billion (ppb) levels.

Generally, Metal oxide semiconductor sensors are available on the market. The operational temperature of such sensor system is high. The performance (sensitivity and selectivity) of the sensor is significant [53-55]. The Scientific community is focused to work on room temperature operated sensor system. Some reports are available on conducting polymer based sensors. It is operated at room temperature. The advantages of the sensor materials are sensitive layer of gases, intrinsic conductivity, fast response, low cost, light weight, ease of synthesis, stability in air and particularly, their sensitivity at the room temperature [56-58]. In conducting polymer family, one of the members is polyaniline. It is exist in two forms. Former is called polyaniline emeraldine base and is insulating ($\sigma \sim 10^{-5}$ S/cm) nature. Later one is polyaniline emeraldine salt and is metallic nature ($\sigma < 1000$ S/cm). The metallic nature is acquired by doping process [59-64]. Two forms of polyaniline polymer are completely different their chemical and physical properties. Several reports are available to CO sensing mechanism of polyaniline based sensor materials [65-68]. There is a partial charge transfer from polyaniline nitrogen atom to carbon atom of CO molecules, which leads to an alternation in the conductivity of a conducting polymer [65-68]. So, the possible sensing mechanism is shown in the Figure 12 [66, 68].

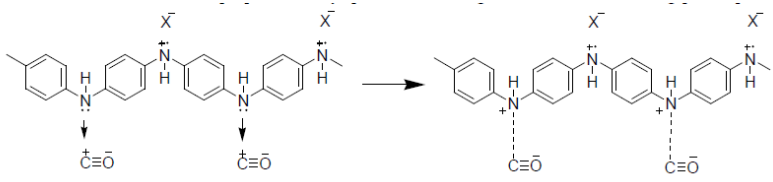

Figure 12. [78, 80] Possible carbon monoxide and polyaniline gas sensing mechanism

The chemistry of partial charge transfer from amine nitrogen: –NH– which have lone pair of electrons to stable resonating structure of +C≡O− having the positive charge at the carbon atom. Hence, the positive charge at the carbon atom is shifted to amine nitrogen atom. It results in a net increase in positive charge carriers on the polymer backbones. Therefore, conductivity of the material in increased. A summary

of health problems caused by exposure to CO is presented in Table 5 and brief summary of conducting polymer based CO detection is mentioned in Table 6.

Table 5. Health problems according to carbon monoxide (CO) concentration and exposure time

Concentration of CO (Exposure Time)	**Created health problems**
35 ppm (6-8 h), 100-200 ppm (2-3 h), 400 ppm (1-2 h), 800 ppm (45 min), 1600 ppm (20 min), 3200 ppm (5-10 min), 6400 ppm (1-2 min)	Headache, dizziness, nausea, loss of judgement and convulsions
1600 ppm (2h)3200 ppm (30min.), 6400 ppm (less than 20 min.), 12,800 ppm (less than 3 min.)	Respiratory arrest, severe conditions (coma) and death

Table 6. Brief summary of CO detection

Study	Materials	Perporfamce	Optimum temperature (^{0}C)	Limitation
Zhao et al.[69]	Polyaniline coated nanofiber	Response time 20 s	Room temperature	Low concentration CO
Liu et al. [70]	polyaniline nanofiber	Response 400 s	Room Temperature	Low CO concentration
Jian et al. [71]	Polyaniline/SnO_2 Nanocomposite	Response time 160 s	Room Temperature	Low CO concentration
Ram et al. [72]	Ultrathin conducting polymer/metal oxide (SnO_2 and/or TiO_2) films	Response time 60 s	Room Temperature	High CO concentration

Conclusions

At room temperature, HCl doped DL−PLA/PANI composites were successfully prepared by *in situ* polymerization technique. SEM characterization reveals that the prepared composites were showed fibrous morphology. ATR−FTIR spectroscopic experiment of DL−PLA polymer and PANI salt indicate that the main chemical structures are identical to those of DL−PLA polymer, the emeraldine salt form of PANI while DL−PLA/PANI nanofibers point to the combination of DL−PLA polymer and PANI salt. UV−Vis's spectra measurements show that the electronic transitions of prepared materials are indicated the emeraldine salt form of PANI on DL−PLA film. Room temperature DC conductivity of prepared composites has shown ohmic behaviour and its value was found to be higher for 2 (M) HCl doped DL−PLA/PANI composite (0.1628×10^{-2} S/cm) than prepared other composites. In addition, we measured DC conductivity as a function of temperature (70−300 K) of

HCl doped DL−PLA/PANI composites and obeyed semiconducting behaviour. Conduction mechanism was studied using temperature dependence of the DC conductivity experiment. In this experiments, metallic (T > 110 K) and localised systems (T<110 K) were observed. The conductivity was found to be controlled by the electron−electron scattering and electron−phonon scattering in case of metallic and localised character, respectively. The temperature dependence magnetoresistivity of HCl doped DL−PLA/PANI composites were performed in the range of 70−300 K at 0.5 T to estimate the L_{loc} of 31.20 nm, 146 nm, and 87.80 nm for 1 (M)−, 2 (M)−, and 3 (M) HCl−doped DL−PLA/PANI composites, respectively. As well, we calculated important transports parameters like $N(E_F), T_{Mott}, L_{loc}, R_{hop}, and\ \Delta_{hop}$ for better understanding of conducting process. The main results obtained from MC are summarized as follows: (1) The sign of MC in the prepared composite films is negative at different temperatures i.e. 50 K, 100 K, 200 K, 300 K in the range of magnetic field (0.1−0.7 tesla). The negative MC increases with lowering temperature. (2) The negative MC is discussed in terms of a quantum interference effect in hopping conduction process. These results suggest that the MC in the composite films made of is controlled by a random network of inter−fibril contacts. Moreover, the prepared composites show features of coherent transport of electrons that persist until high temperatures, making them attractive for further investigations aimed at development of novel devices. In summary, the present work reports the preparation, detailed morphological and spectral, electrical properties with mechanism of HCl doped DL−PLA/PANI composites. In particulars, carbon monoxide gas responses and mechanism of polyaniline-based materials were studied.

Acknowledgements

The author conveys their sincere thanks to the CRF, IIT Kharagpur for their providing testing facilities and Materials Science Centre to do the research work. I would like to thank Prof. Debabrat Pradhan for their invaluable guidance, advices, constant inspiration and technical support throughout the entire research program.

References

[1] Abidia**n**, M.R., Kim, D.H., and Martin, D.C. 2006, Conducting Polymer Nanotubes for Controlled Drug Release**,** Advanced Materials, Vol. 18, pp. 405-409.

[2] Komarova, E., Aldissi, M., and Bogomolova, A. 2005, Direct Electrochemical Sensor for Fast Reagent−Free DNA Detection, Biosensor and Bioelectronics, Vol. 21, pp. 182-189.

[3] Ohtani, A., Abe, M., Ezoe, M., Doi, T., Miyata, T., and Miyake, A., 1993, Synthesis and Properties of High−Molecular−Weight Soluble Polyaniline and its Application to the 4mb−Capacity Barium Ferrite Floppy Disks Antistatic Coating, Synthetic Metals, Vol. 57, pp. 3696-3701.

[4] Gustafsson, G., Cao, Y., Treacy, G.M., Klavetter, F., Colaneri, N., and Heeger, A.J. 1992, Flexible Light−Emitting Diodes Made from Soluble Conducting Polymers, Nature, Vol. 357, pp. 477-479.

[5] Rudge, A., Raistrick, I., Gottesfeld, S., and Ferraris, J.P. 1994, A Study of the Electrochemical Properties of Conducting Polymers for Application in Electrochemical Capacitors, Electrochemical Acta, Vol. 39, pp. 273-287.

[6] Ryu, K.S., Kim, K.M., Kang, S.G., Lee, G. J., Joo, J., and Chang, S.H. 2000, Electrochemical and Physical Characterization of Lithium Ionic Salt Doped Polyaniline as a Polymer Electrode of Lithium Secondary Battery, Synthetic Metas, Vol.3, pp. 213-217.

[7] MacDiarmid, A.G., and Zheng, W.G. 1997, Electrochemistry of Conjugated Polymers and Electrochemical Applications, Materials Research Society Bulletin, Vol. 22, pp. 24-30.

[8] Sathiyanarayanan, S., Dhawan, S.K., Trivedi, D.C., and Balakrishnan, K.1992, Soluble Conducting Poly Ethoxy Aniline as an Inhibitor for Iron in HCl, Corrosion Science, Vol. 33, pp. 1831-1841.

[9] Kaneto, K., Kaneko, H., Takashima, W.J., 1995, Response of Chemomechanical Deformation in Polyaniline Film on Variety of Anions, Japanese Journal of Applied Physics, Vol. 34, pp. 837- 840.

[10] Aliwi, S.M., Hassan, A.K., 2008, Interaction of Thin Films of Hydroxo−Oxobis (8−Quinolyloxo) Vanadium (V) with Ammonia Vapour, Sensor and Actuators B, Vol. 133, pp. 521-525.

[11] M. S. Cho, S. Y. Park, J. Y. Hwang, H. J. Choi, 2004, Synthesis and Electrical Properties of Polymer Composites with Polyaniline Nanoparticles, Materials Science and Engineering C, Vol. 24, pp. 15-18.

[12] Diaz, A.F., and Logan, J.A. 1980, Electroactive Polyaniline Films, Journal of Electroanalytical Chemistry, Vol. 111, pp. 111-114.

[13] Cao, Y., Andreatta, A., Heeger , A.J., Smith, P. 1989, Influence of Chemical Polymerization Conditions on the Properties of Polyaniline, Polymer, Vol. 30, pp. 2305-2311.

[14] Kingsborough, R.P., and Swager, T.M. 1998, Electroactivity Enhancement by Redox Matching in Cobalt Salen–Based Conducting Polymers, Advanced Materials, Vol. 10, pp. 1100-1104.

[15] Omastova, M., Pavlinec, J., Pionteck, J., Simon, F., and Kosina, S. 1998, Chemical Preparation and Characterization of Conductive Poly(Methyl Methacrylate)/Polypyrrole Composites, Polymer, Vol. 39, 6559-6566.

[16] Nikpour, M., Chaouk, H., Mau, A., Chung, D.J., and Wallace, G., 1999, Porous Conductive Films based on Polypyrrole−PMMA Composites, Synthetic Metals, Vol. 99, pp. 121-126.

[17] Cairns, D.B., Armes, S.P., and Bremer, L.G.B. 1999, X−ray Photoelectron Spectroscopy Characterization of Submicrometer−Sized Polypyrrole−Polystyrene Composites, Langmuir, Vol. 15, pp. 8052-8058.

[18] He, F., Omoto, M., Yamamoto, T., and Kise, H.1995, Preparation of Polypyrrole− Polyurethane Composite Foam by Vapour Phase Oxidative Polymerization, Journal of Applied Polymer Science, Vol. 55, pp.283-287.

[19] Huang, L., Hu, J., Lang, L., Wang, X., Zhang, P., Jing, X., Wang, X., Chen, X., Lelkes, P.I., MacDiarmid, A.G., and Wei, Y. 2007, Synthesis and Characterization of Electroactive and Biodegradable ABA Block Copolymer of Polylactide and Aniline Pentamer, Biomaterials, Vol. 28, pp. 1741-1751.

[20] Tuan VO−DINH, T. 2004, biosensors, nanosensors and biochips: Frontiers in Environmental and Medical Diagnostics, the 1st International Symposium on Micro & Nano Technology, 14−17 march, 2004, Honolulu, Hawaii, USA.

[21] Shi, G., Rouabhia, M., Wang, Z., Dao, L.H., and Zhang, Z. 2004, A Novel Electrical Conductive and Biodegradable Composite Made of Polypyrrole and Polylactide, Biomaterials, Vol. 25, pp. 2477-2488.

[22] Aleshin, A.N., Williams, S.R., and Heeger, A.J. 1998, Transport Properties of Poly(3, 4-ethylenedioxythiophene)/Poly(styrenesulfonate), Synthetic Metals, Vol. 94, pp. 173-177

[23] Duvail, J.L., Retho, P., Garreau, S., Lauran, G., Godon, C., and Demoustier−Champagen, S. 2002, Transport and Vibrational Properties of Poly(3,4-Ethylenedioxythiophene) Nanofibers, Synthetic Metals, Vol. 131, pp. 123-128.

[24] Skotheim T.A., Elsenbaumer RL, and Reynolds J.R. 1998 Handbook of Conducting Polymers 2nd edn (New York: Dekker) pp 27-121.

[25] Kaiser, A.B. 2001, Electronic Transport Properties of Conducting Polymers and Carbon Nanotubes, Reports on Progress in Physics, Vol**.** 64, pp. 1-49.

[26] Coehoorn, R. Lecture Notes 2003, Novel Magnetoelectronic Materials and Devices, Exchange−Biased Spin−Valves.

[27] Ghosh, M., Barman, A., Meikap, A.K., De, S.K., Chatterjee, S. Chattopadhyay, S.K. 2000, Electrical Resistivity and Magnetoresistivity of Protonic Acid (H_2SO_4 and HCl)−Doped Polyaniline at Low Temperature, Journal of Applied Polymer Science, Vol. 75, pp. 1480-1486.

[28] Chiquito, A.J., Lanfredi, A.J.C., Oliveira, R.F.M. de, Pozzi, L.P. and Leite, Ed. R. 2007, Electron Dephasing and Weak Localization in Sn Doped In_2O_3 Nanowires, Nano letter, Vol. 7, pp. 1439-1443.

[29] Taunk, M., Kapil, A., and Chand, S. 2008, Synthesis and Electrical Characterization of Self−Supported Conducting Polypyrrole−Poly (vinylidene fluoride) Composite Films, The Open Macromolecular Journal,

Vol. 2, pp. 74-79.

[30] Zhang, Z. , Wei, Z., Wa, M. 2002, Nanostructures of Polyaniline Doped with Inorganic Acids, Macromolecules, Vol. 35, pp. 5937-5942.

[31] Mukherjee, K., Majumdar, S.B., 2009, Analyses of Response and Recovery Kinetics of Zinc Ferrite as Hydrogen Gas Sensor, Journal of applied Physics, Vol. 106, pp. 064912-064922.

[32] Huang, J.W., Hung, Y.C., Wen, Y.L., Kang, C.C., and Yeh, M.Y. 2009, Polylactide/Nano and Microscale Silica Composite Films. I. preparation and characterization, Journal of Applied Polymer Science, Vol. 112, pp. 1688-1694.

[33] Arenas, M.C., Andablo, E., and Castaño, V.M. 2010, Synthesis of Conducting Polyaniline Nanofibers from Single and Binary Dopant Agents, Journal of Nanoscience and Nanotechnology, Vol. 10, pp. 549-554.

[34] Shameli, K., Ahmad ,M. Bin, Md Zin Wan Yunus, W., Ibrahim, N.A., Jokar, M., Darroudi, M. 2010, Synthesis and Characterization of Silver/Polylactide Nanocomposites, World Academy of Science, Engineering and Technology, Vol. 64, pp. 28-32.

[35] Tzou, K., and Gregory, R.V. 1993, a Method to Prepare Soluble Polyaniline Salt Solutions−*in situ* Doping of PANI Base with Organic Dopants in Polar Solvents, Synthetic Metals, Vol. 53, pp. 365-377.

[36] Lossy, R., Pappas, D.L., Roy, R.A., and Cuomo, J.J., and Sura, V.M. 1992, Filtered Arc Deposition of Amorphous Diamond, Applied Physics Letter, Vol. 61, pp. 171-173.

[37] Li, J., Fang, K., Qiu, H., Li, S., and Mao, W. 2004, Micromorphology and Electrical Property of the HCl−Doped and DBSA-Doped Polyaniline, Synthetic Metals, Vol. 142, pp. 107-111.

[38] Shameli, K., Ahmad, M. Bin, Wan Yunus, W. Md Zin, Ibrahim, N.A., Jokar, M., and Darroudi, M. 2010, Synthesis and Characterization of Silver/Polylactide Nanocomposites, World Academy of Science, Engineering, and Technology., Vol. 64, pp. 28-32.

[39] (50) Sinha, S., Bhadra, S., and Khastagir, D.J. 2009, Effect of Dopant Type on the Properties of Polyaniline, Journal of Applied Polymer Science, Vol. 112, pp. 3135-3140.

[40] Thornton, T.J., Roukes, M.L., Scherer, A., and Van der Gaag, B.P. granular nanoelectronics; Ferry, D.K., and Baker, J R. Eds. C. Jacoboni, NATO ASI Series; Plenum Press: New York, 1991.

[41] Berengue, O.M., Chiquito, J., Pozzi, L.P., Lanfredi, A.J. de Castro, and Leite, E.R. 2009, Electron-Phonon Scattering in Sn-Doped In_2O_3 FET Nanowires Probed by Temperature-Dependent Measurements,

Nanotechnology, Vol. 20, pp. 245706-xxx.

[42] Lin, J.J. and Bird, J.P. 2002, Recent Experimental Studies of Electron Dephasing in Metal and Semiconductor Mesoscopic Structures, Journal of Physics: Condensed Matter, Vol. 14, pp. R501–R596.

[43] Chakraborty, G., Gupta, K., Meikap, A.K., and Jana, P.C. 2010, Direct Current Electrical Transport and Magneto Transport Properties of Polyaniline Nanocomposites, Journal of Physical Science, Vol. 14, pp.207-218.

[44] Long, Y., Chen, Z., Shen, J., Zhang, Z., Zhang, L., Huang, K., Wan, M., Jin, A., Gu, C., and Duvail, J.L. 2006, Magnetoresistance Studies of Polymer Nanotube/Wire Pellets and Single Polymer Nanotubes/Wires, Nanotechnology, Vol. 17, pp. 5903–5911.

[45] Wang, Z.H., Javadi, H.H.S., Ray, A., Macdiarmid, A.G., and Epstein, A. J. 1990, Electron Localization in Polyaniline Derivatives, Physical Review B (Rapid communication), Vol. 42, pp. 5411-5414.

[46] Li, W., and Wan, M. 1998, Porous Polyaniline Films with High Conductivity, Synthetic Metals, Vol. 92, pp. 121-126.

[47] Beutler, D.E., and Giordano, N. 1988, Localization and Electron−Electron Interaction Effects in Thin Bi Wires and Films, Physical Review, B, Vol. 38, pp. 8-19.

[48] Nandy, T., Coutu, R.A., and Ababei, C., 2018, Review Carbon Monoxide Sensing Technologies for Next-Generation Cyber-Physical Systems, Sensors, Vol. 18, p. 3443-3469.

[49] Varon, J., Marik, P.E., Fromm, R.E., Jr.. and Gueler, A. 1999, Carbon Monoxide Poisoning: a Review for Clinicians, Journal of Emergency Medicine, Vol. 17, pp. 87-93.

[50] Raub, J.A., Mathieu-Nolf, M., Hampson, N.B., and Thom, S.R. 2000, Carbon Monoxide Poisoning-A Public Health Perspective, Toxicology, Vol. 145, pp. 1-14.

[51] Respiratory Health–Air Pollution, Boston University School of Public Health. Available online:http://sphweb.bumc.bu.edu/otlt/MPH-Modules/ PH/ Respiratory Health/ Respiratory Health 7.html (accessed on 28 September 2018).

[52] Harper, A. and Croft-Baker, J. 2004, Carbon Monoxide Poisoning: Undetected by both Patients and Their Doctors, Age Ageing, Vol. 33, pp. 105-109.

[53] Goldstein, M. 2008, Carbon Monoxide Poisoning, Journal of Emergency Nursing, Vol. 34, pp. 538-542.

[54] Pijolat, C., Pupier, C., Sauvan, M., Tournier, G., and Lalauze, R.1999, Gas Detection for Automotive Pollution Control, Sensor and Actuators B, Vol. 59, pp. 195-202.

[55] Meixner, H., Gerblinger, J., Lampe, U., and Fleischer, M. 1995, Thin-Film Gas Sensors based on Semiconducting Metal Oxides, Sensor and Actuators B, Vol. 23, pp. 119-125.

[56] Lim, J.-W., Kang, D.-W., Lee, D.-S., Huh, J.-S., and Lee, D.-D. 2001, Heating Power-Controlled Micro-Gas Sensor Array, Sensor and Actuators B, Vol. 77, pp. 139-144.

[57] Zhang, W., de Vasconcelos, E.A., Uchida, H., Katsube, T., Nakatsubo, T., and Nishioka, Y. 2000, A Study of Silicon Schottky Diode Structures for NO*x* Gas Detection, Sensor and Actuators B, 65, pp. 154-156.

[58] Rickerby, D.G., Horrillo, M.C., Santos, J.P., and Serrini, P. 1997, Microstructural characterization of nanograin tin oxide gas sensors, Nanostructured Materials, Vol. 9, pp. 43-52.

[59] J. Melendez, A.J. de Castro, F. Lopez, J. Meneses, 1995, Spectrally Selective Gas Cell for Electrooptical Infrared Compact Multi-Gas Sensor, Sensor and Actuators A, Vol. 46–47, pp. 417-421.

[60] McQuade, D.T., Pullen, A.E., and Swager, T.M., 2000, Conjugated Polymer based Chemical Sensors, Chemical Reviews, Vol. 100, pp. 2537-2574.

[61] Monkman, A.P., Petty, M.C., Agbor, N.E., and Scully, M.T. Polyaniline Gas Sensor, US Patent 5536473, 16 July 1996.

[62] Torsi, L., Pezzuto, M., Siciliano, P., Rella, R., Sabbatini, L., Valli, L., and Zambonin, P.G. 1998, Conducting Polymers Doped with Metallic Inclusions: New Materials for Gas Sensors, Sensor and Actuators B, Vol. 48, pp. 362-367.

[63] Chiang, J.C., and MacDiarmid, A.G. 1986, Polyaniline: a New Concept in Conducting Polymers, Synthetic Metals, Vol. 13, pp. 193-xxx.

[64] Dhawan, S.K., Kumar, D., Ram, M.K., Chandra, S., and Trivedi, D.C. 1997, Application of Conducting Polyaniline as Sensor Material for Ammonia, Sensor and Actuators Vol. 40, pp. 99-103.

[65] Paddeu, S., Ram, M.K., and Nicolini, C. 1998, Langmuir–Schaefer Films of a Poly(O-Anisidine) Conducting Polymer for Sensors and Displays, Nanotechnology, Vol. 9, pp. 228-236.

[66] Dixit, V., Misra, S.C.K., and Sharma, B.S. 2005, Carbon Monoxide Sensitivity Of Vacuum Deposited Polyaniline Semiconducting Thin Films, Sensor and Actuators B, Vol. 104, pp. 90-93.

[67] Densakulprasert, N., Wannatong, L., Chotpattananont, D., Hiamtup, P.,

Sirivat, A., and Schwank, J. 2005, Electrical Conductivity Of Polyaniline/Zeolite Composites and Synergetic Interaction with CO, Materials Science and Engineering B-Solid State for Materials Advanced Technology, 117, 276-282.

[68] Misra, S.C.K., Mathur, P., and Srivastava, B.K. 2004, Vacuum-Deposited Nanocrystalline Polyaniline Thin Film Sensors for Detection of Carbon Monoxide, Sensor and Actuators A, Vol. 114, pp. 30-35.

[69] Watcharaphalakorn, S., Ruangchuay, L., Chotpattahanont, D., Sirivat, A., and Schwank, J. 2005, Polyaniline/Polyimide Blends as Gas Sensors and Electrical Conductivity Response to CO-N-2 Mixtures, Polymer International, Vol. 54, pp. 1126-1133.

[70] Zhao, J., Wu, G., Hu, Y., Liu, Y., Tao, X., and Chen, W. 2015, A Wearable And Highly Sensitive Co Sensor with a Macroscopic Polyaniline NanoFiber Membrane, Journal of Materials Chemistry A, Vol. 3, pp. 24333-24337.

[71] Liu, C., Noda, Z., Sasaki, K., and Hayashi, K. 2012, Development of A Polyaniline Nanofiber-based Carbon Monoxide Sensor for Hydrogen Fuel Cell Application, International Journal of Hydrogen Energy, Vol. 37, pp. 13529-13535.

[72] Jian, K.-S., Chang, C.-J., Wu, J.J., Chang, Y.-C., Tsay, C.-Y., Chen, J.-H., Horng, T.-L., Lee, G.-J., Karuppasamy, L., Anandan, S., and Chen, C.-Y. 2019, High Response CO Sensor Based on a Polyaniline/SnO_2 Nanocomposite, Polymers, Vol. 11, pp. 184-200.

[73] Ram, M.K., Yavuz, O.Z., Lahsangah, V., and Aldissi, M. 2005, CO Gas Sensing from Ultrathin Nano-Composite Conducting Polymer Film, Sensors and Actuators B, Vol. 106, pp. 750-757.